Supplementary information

Unveiled effects of methylammonium chloride additives on formamidinium lead halide: Expediting carrier injection from the photoabsorber to carrier transport layers through spontaneously modulated heterointerfaces in perovskite solar cells

Naoyuki Nishimura[*†], Ranjan Kumar Behera[†], Ryuzi Katoh[§], Hiroyuki Kanda[†],*

Takurou N. Murakami[†], Hiroyuki Matsuzaki[*†]*

[†] National Institute of Advanced Industrial Science and Technology (AIST),1-1-1 Higashi, Tsukuba, Ibaraki 305-8565, Japan.

[§] College of Engineering, Nihon University, Koriyama, Fukushima 963-8642, Japan

Corresponding Author

Naoyuki Nishimura, E-mail: naoyuki-nishimura@aist.go.jp

Hiroyuki Matsuzaki, E-mail: hiroyuki-matsuzaki@aist.go.jp

1. Experimental methods

1-1. Materials

All materials were reagent grade and used as-purchased. 2-methoxyethanol, ethanol were purchased from WAKO-Chemicals Co. Ltd.. Formamidine hydroiodide (FAI), lead iodide (PbI_2), methylammonium chloride (MACl), 4-*tert*-butylpyridine (TBP) were purchased from Tokyo Chemical Industry Co. Ltd.. Mesoporous titanium oxide (m-TiO_2; 18NR-T) precursor was from Great Cell Solar. 2,2',7,7'-tetrakis-(*N,N*-di-4-methoxyphenylamino)-9,9'-spirobifluorene (Spiro-OMeTAD) was from Nippon Fine Chemical Co.. Other reagents were from Sigma Aldrich. Fluorine-doped tin oxide (FTO) coated transparent glass (thickness: 1.6 mm, sheet resistance $\leq 10 \ \Omega \ cm^{-2}$) was purchased from Nippon Sheet Glass.

1-2. Synthesis of FAPbI₃ powder

$FAPbI_3$ powder was synthesized as the precursor of the thin film by the previously reported method.[1,2,3] 0.8 M of FAI and PbI_2 powders were dissolved into 2-methoxyethanol, and then the solution was heated at 393 K for 1 h under stirring. Subsequently, the precipitated black particles were immediately collected by filtration, and subsequently heated at 423 K for 30 min. Finally, the resulting powder was further dried under evacuation at room temperature for 1 h.

1-3. Solar cell fabrication

The PSCs were prepared by the conventional methods[1,2,3] with minor modifications. TiO_2 compact layer with thickness of ~50 nm was coated onto FTO glass substrate, which was placed on hotplate at 523 K, by spray pyrolysis using 7.5 vol% of titanium diisopropoxide bis(acetylacetate)/ethanol solution. After that, a mesoporous TiO_2 (*m*-TiO_2) layer was deposited by spin coating of TiO_2 paste diluted with ethanol onto the substrate at 2000 rpm for 30 s, followed by heating the substrate at 773 K for 30 min.

$FAPbI_3$ perovskite layer was deposited on the prepared TiO_2/FTO by spin coating in a dry room (temperature: 291 K, dew point: <243 K). 1.8 M of $FAPbI_3$ precursor solution was prepared by dissolving the synthesized $FAPbI_3$ powder (and 40 mol% for $FAPbI_3$ of MACl) into mixed solution of *N,N*-dimethylformamide and dimethyl sulfoxide (4:1 vol ratio). The TiO_2/FTO substrate was spin-coated with the perovskite precursor solution at 6000 rpm for 50 s. During the spin coating, 1 mL of chlorobenzene (CB) was dropped after spinning for 10 s. For some samples, OAI passivation over the as-prepared $FAPbI_3$ layer was employed in the dry room; OAI/ isopropyl alcohol solution was spin-coated over the $FAPbI_3$ layer, followed by heating at 373 K for 5 min. The layer of the hole-transport material (HTM) was deposited by spin coating of the solution containing Spiro-OMeTAD and additives at 3000 rpm for 30 s in the dry room. The HTM solution was prepared by dissolving 70 mM Spiro-OMeTAD, 0.27 mM tBP, followed by mixing the stock acetonitrile solutions of bis(trifluoromethane) sulfonamide lithium salt and tris(2-(1H-pyrazol-1-yl)-4-tertbutylpyridine)-

cobalt(III)tris(bis(trifluoromethylsulfonyl)imide (FK209) to be 35 mM and 4.2 mM, respectively.

Finally, gold (Au) conductor layer with thickness of ~200 nm was deposited via thermal evaporation.

1-4.   External quantum efficiency spectra

The external quantum efficiency (EQE) action spectra were measured by with an action spectrum

measurement setup (CEP-99W, Bunkou Keiki).

1-5.   Characterization of perovskite films

The compositional depth profile was measured by secondary ion mass spectroscopy (SIMS; PHI,

ADEPT1010) with primary cation of Cs^+ and detection mode of negative ions. The depth was

estimated with the sputter rate of each layer. X-ray diffraction patterns were obtained with X-ray

diffractometer (Smartlab, Rigaku) with a Cu Kα radiation source. The UV-vis absorption spectra for

the bandgap estimation were measured with a spectrophotometer (UV3600, Shimazu). The scanning

electron microscope (SEM) images were obtained with an equipment (SU9000, Hitachi)
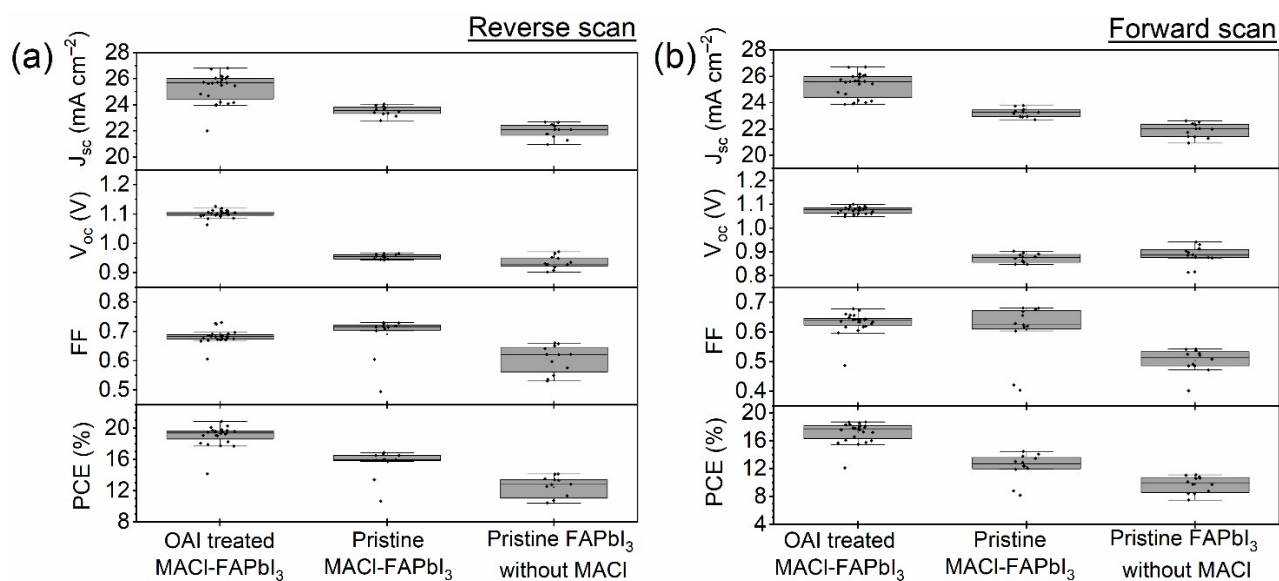
2. PV performances

Fig. S1 Distributions of PV parameters

Table S1. Averaged PV parameters

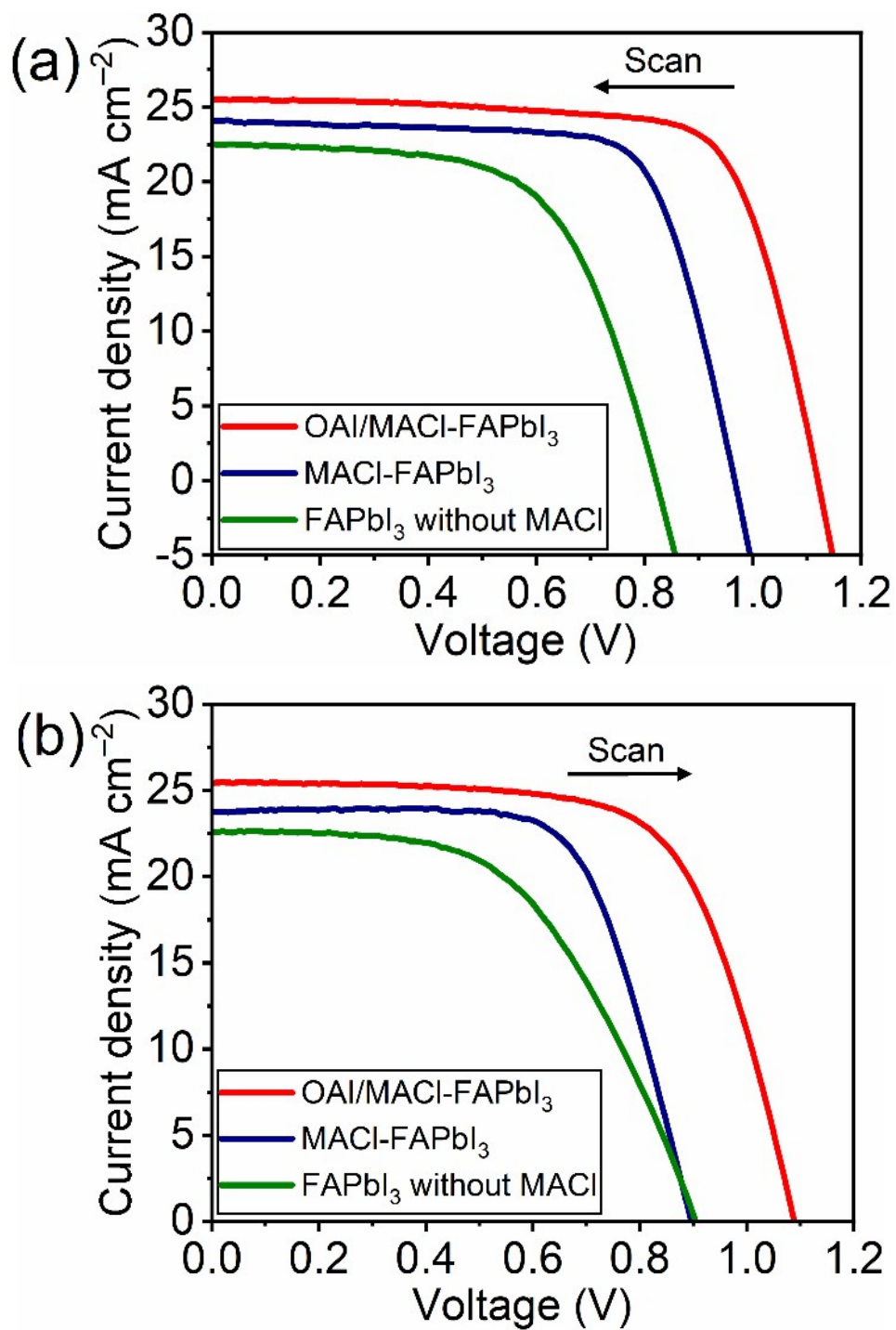| Sample	Scan	Jsc (mA/cm^2)	Voc (V)	FF	PCE (%)
OAI treated MACl-FAPbI$_3$	Reverse	25.3 ± 1.1	1.10 ± 0.01	0.68 ± 0.02	19.0 ± 1.3
	Forward	25.3 ± 0.9	1.08 ± 0.01	0.63 ± 0.04	17.2 ± 1.4
Pristine MACl-FAPbI$_3$	Reverse	23.5 ± 0.3	0.96 ± 0.01	0.69 ± 0.07	15.5 ± 1.7
	Forward	23.3 ± 0.3	0.87 ± 0.02	0.61 ± 0.09	12.3 ± 1.9
Pristine FAPbI$_3$ without MACl	Reverse	22.0 ± 0.5	0.94 ± 0.02	0.61 ± 0.04	12.5 ± 1.3
	Forward	21.9 ± 0.5	0.88 ± 0.04	0.50 ± 0.04	9.8 ± 1.2

Fig. S2 Current density-voltage (J-V) curves (a) in reverse and (b) forward scans of the PSCs employed
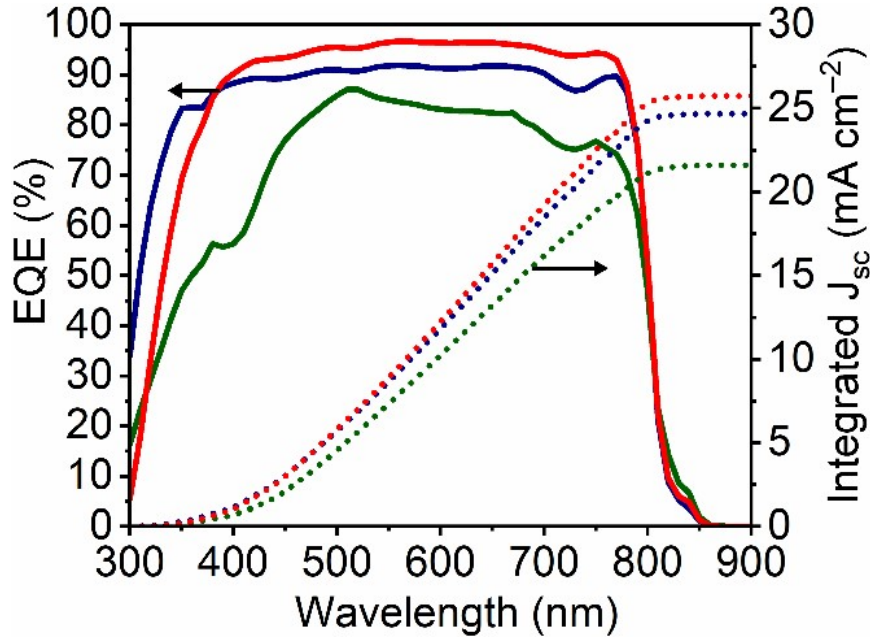
in the TRPLS measurements

Fig. S3 EQE spectra of the PSCs employed in the TRPLS measurements, consisting of photoabsorbers of MACl-FAPbI$_3$ with OAI passivation (red), pristine MACl-FAPbI$_3$ (blue), pristine FAPbI$_3$ without MACl (green)

The integrated J$_{sc}$ estimated from the EQE curves were 25.7 mA cm^{-2}, 24.7 mA cm^{-2}, and 21.6 mA cm^{-2} for OAI passivation, pristine MACl-FAPbI$_3$, pristine FAPbI$_3$ without MACl, respectively. Thus, the estimated values well matched to the ones in J-V curves (Table 1); the differences of J$_{sc}$ in J-V curves (Table 1) from these integrated J$_{sc}$ were +1%, +3%, and −5% for OAI passivation, pristine MACl-FAPbI$_3$, pristine FAPbI$_3$ without MACl, respectively.

3. Characterizations of the photoabsorber layers

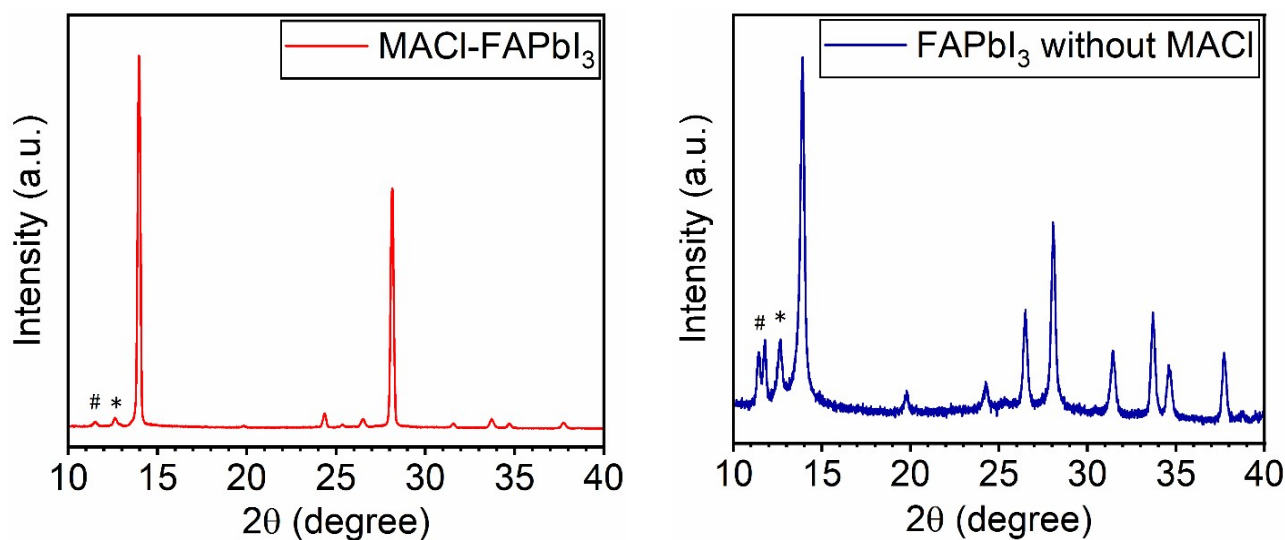## 3-1. Crystal structure changes

Fig. S4 XRD patterns of MACl-FAPbI$_3$ and FAPbI$_3$ without MACl

The XRD peaks labeled by * and # in Fig. S4 correspond to the peaks originated from PbI$_2$ and hexagonal FAPbI$_3$, which are impurity phases that possess too large bandgaps to functions as photoabsorber. The MACl additive render these impurity phases considerably less so contributed to the improvement of the PV performances (Table 1, Fig. S1–S3)
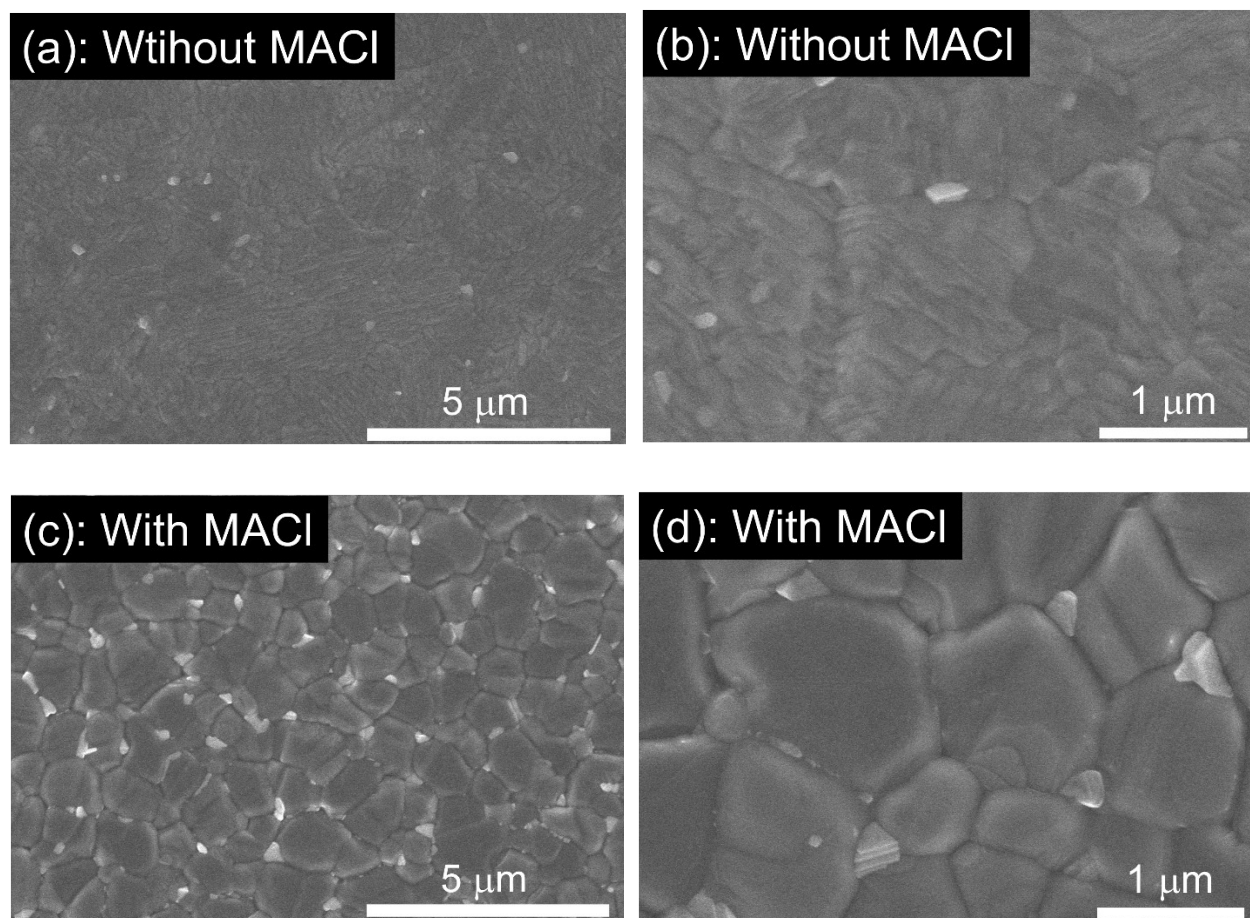
3-2. Morphological changes

Fig. S5 Top view of SEM images of (a) FAPbI$_3$ without MACl ((b) zoomed in), and (c) MACl-FAPbI$_3$

((d) zoomed in)

The top views of MACl-FAPbI$_3$ samples shown in Fig. S5 exhibited clear crystal habits that the sample

without MACl did not possess. This morphological change strongly suggests that MACl additive

facilitated crystal growth of FAPbI$_3$.
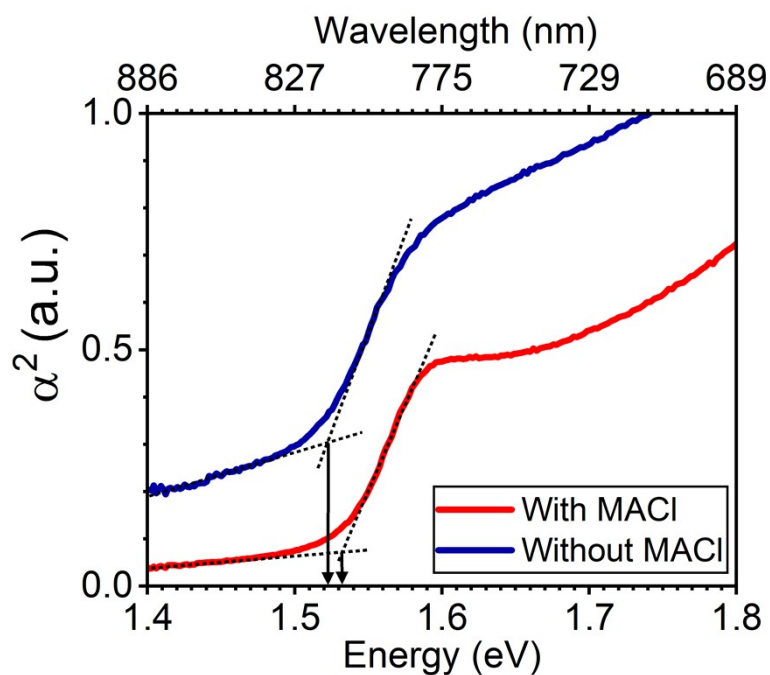
3-3. Optical bandgaps

Fig. S6 UV-vis absorption spectra of MACl-FAPbI$_3$ and FAPbI$_3$ without MACl and the corresponding

absorption-edge energy

Optical density of each monolayer film is employed as α value in Fig. S6. The MACl addition changed

bandgap energy of FAPbI$_3$ a little; both samples possessed bandgap energy of around 1.53 eV.
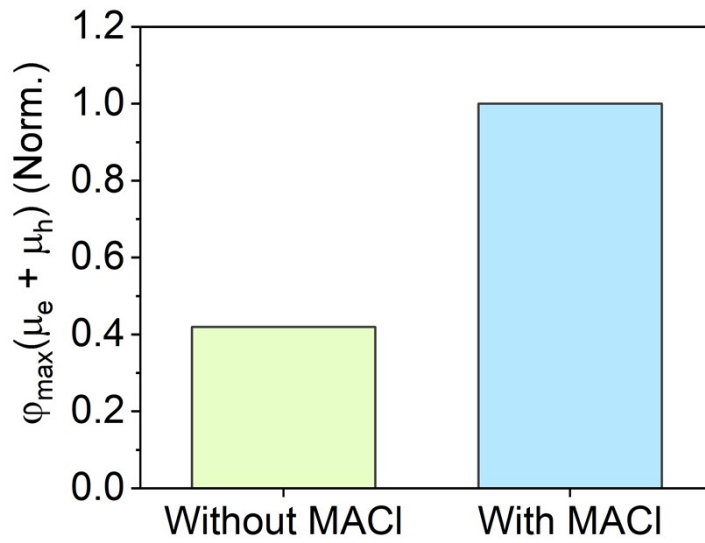
3-4. Carrier mobilities

Fig. S7 Relative carrier mobilities of FAPbI$_3$ monolayer samples with or without MACl estimated from initial intensities in the TRMC signals ($\varphi_{max}(\mu_e + \mu_h)$)

Initial intensities in the TRMC signals, which is the maximum value, for the perovskite/quartz monolayer samples indicate the relative value of sum of carrier mobility of electron and hole in the perovskite layers (eqn S4 in the section 7 shown later). MACl addition increased the sum of carrier mobility in FAPbI$_3$ by approximately 2.5 times.

4. Analysis of the excitation power dependence on the PL lifetimes

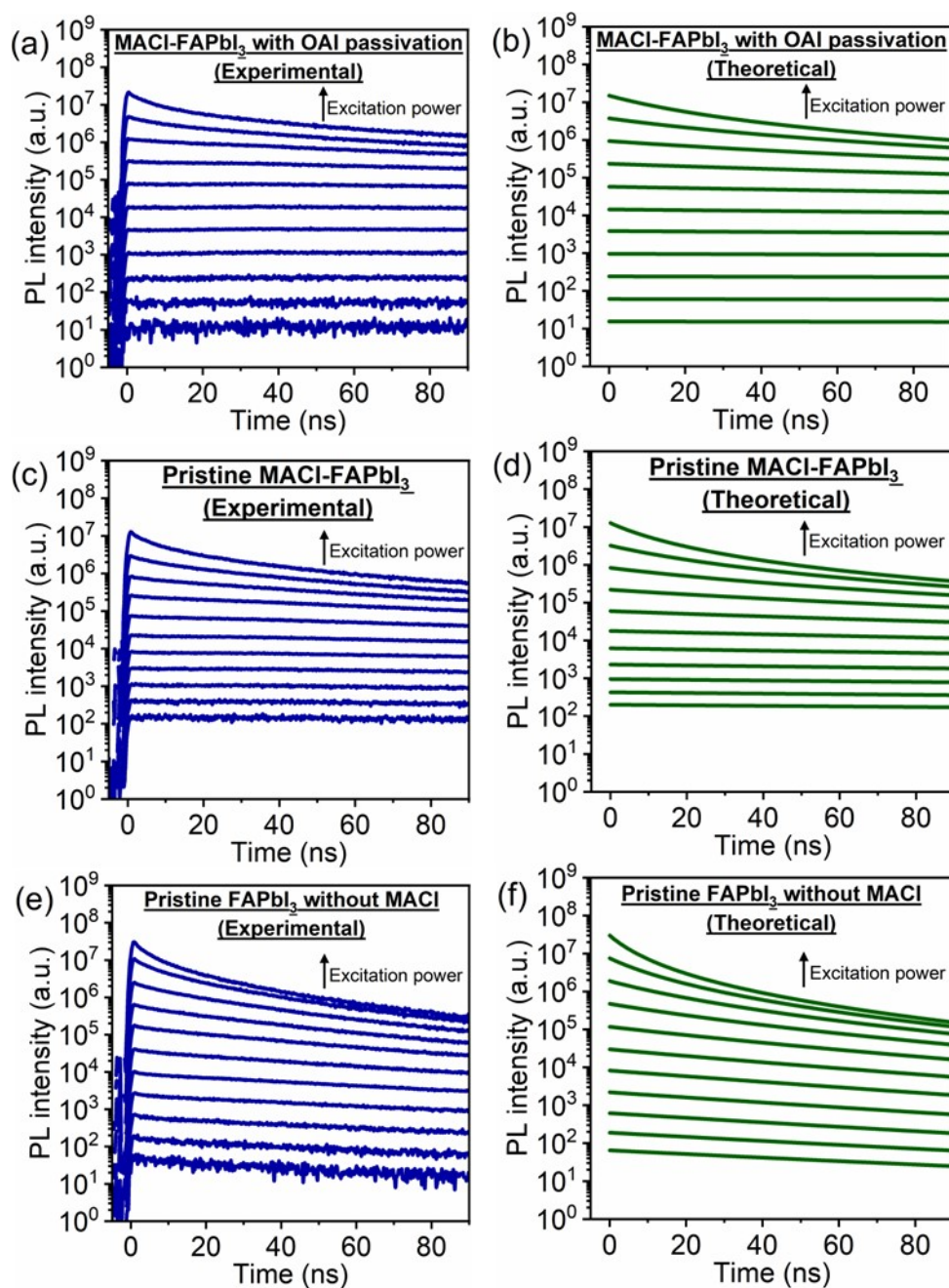## 4-1. PL decays of perovskite monolayer samples

Fig. S8 Experimental and theoretical excitation power dependence on the PL decay (1–1000 nJ cm^{-2}/pulse: 1, 2, 4, 8, 16, 31, 62, 125, 250, 500, and 1000 nJ/cm^2) of perovskite monolayers of (a) MACl-FAPbI$_3$ with OAI passivation, (b) pristine MACl-FAPbI$_3$, (c) pristine FAPbI$_3$ without MACl

4-2. Kinetics parameter fitting

For the kinetics parameter fittings of A, B, C values, A and B values were firstly estimated with the PL lifetime and intensity of the monolayer samples (shown in below Fig. S9), and then, the C values were calculated by approximating the best fit with the PL lifetime trend of the solar cells using each A and B value corresponding to the photoabsorbers. (Fig. S10) Origin© software for data plotting and wolfram mathematica (11.3 version) was used for the theoretical data fitting. The PL intensity is equated by the following relation.

$$I_{Pl} \propto Bn^2 + BNn \qquad (S1)$$

Here, N represent the unintentional doping in the sample. The initial photoexcited carrier density n_0 (t = 0) at 1 nJ fluence is 1.46×10^{15} cm^{-3} for MACl-FAPbI$_3$ with OAI passivation, and 1.33×10^{15} cm^{-3} for pristine MACl-FAPbI$_3$, and pristine FAPbI$_3$ without MACl samples. This is calculated by using the beam profile of excitation light at the sample position and absorption coefficient (3.33×10^4 cm^{-1}) of the perovskite materials at 650 nm[4].
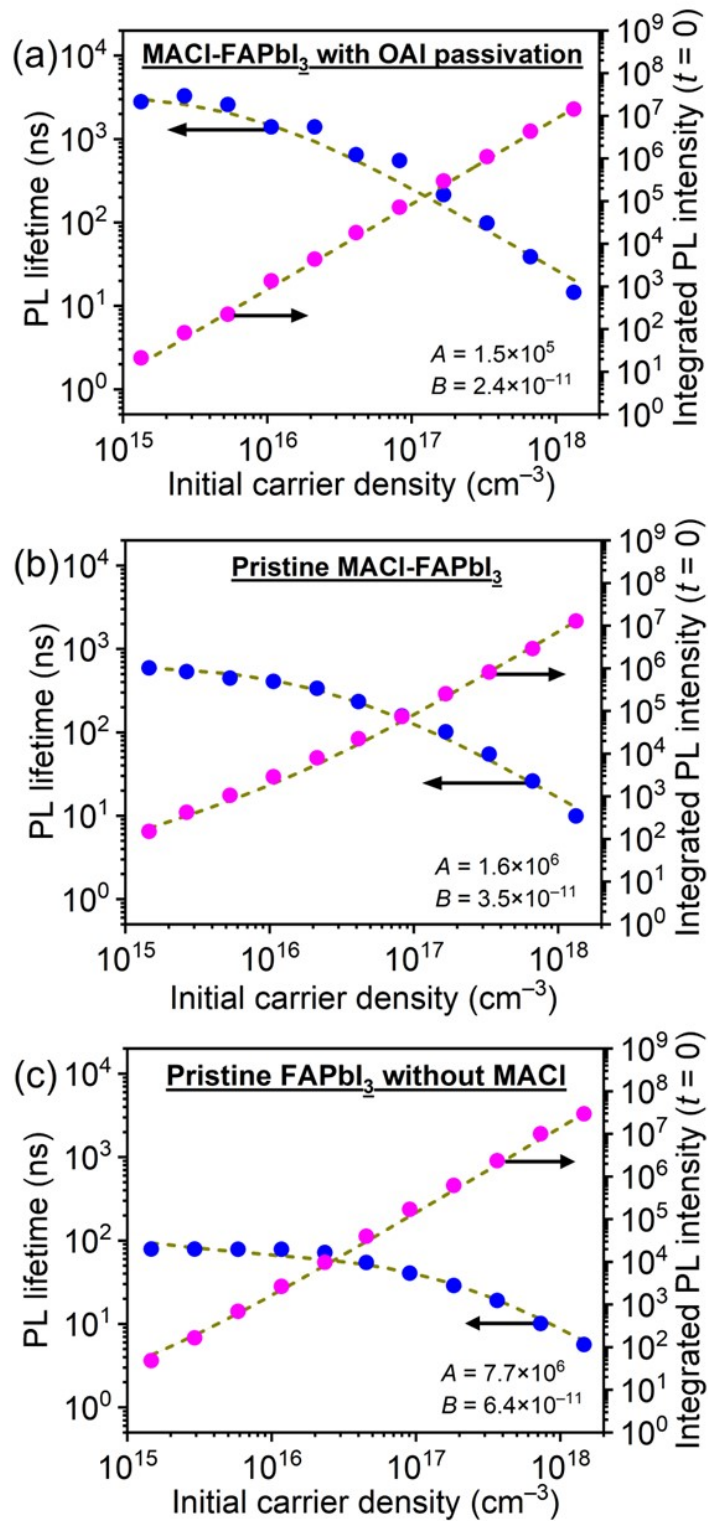
13

Fig. S9 Excitation power dependence on the PL lifetime (blue) and integrated PL intensity ($t = 0$, magenta) of perovskite monolayer samples of (a) MACl-FAPbI$_3$ with OAI passivation, (b) pristine MACl-FAPbI$_3$, and (c) pristine FAPbI$_3$ without an MACl. The dashed lines denote fitting curves.
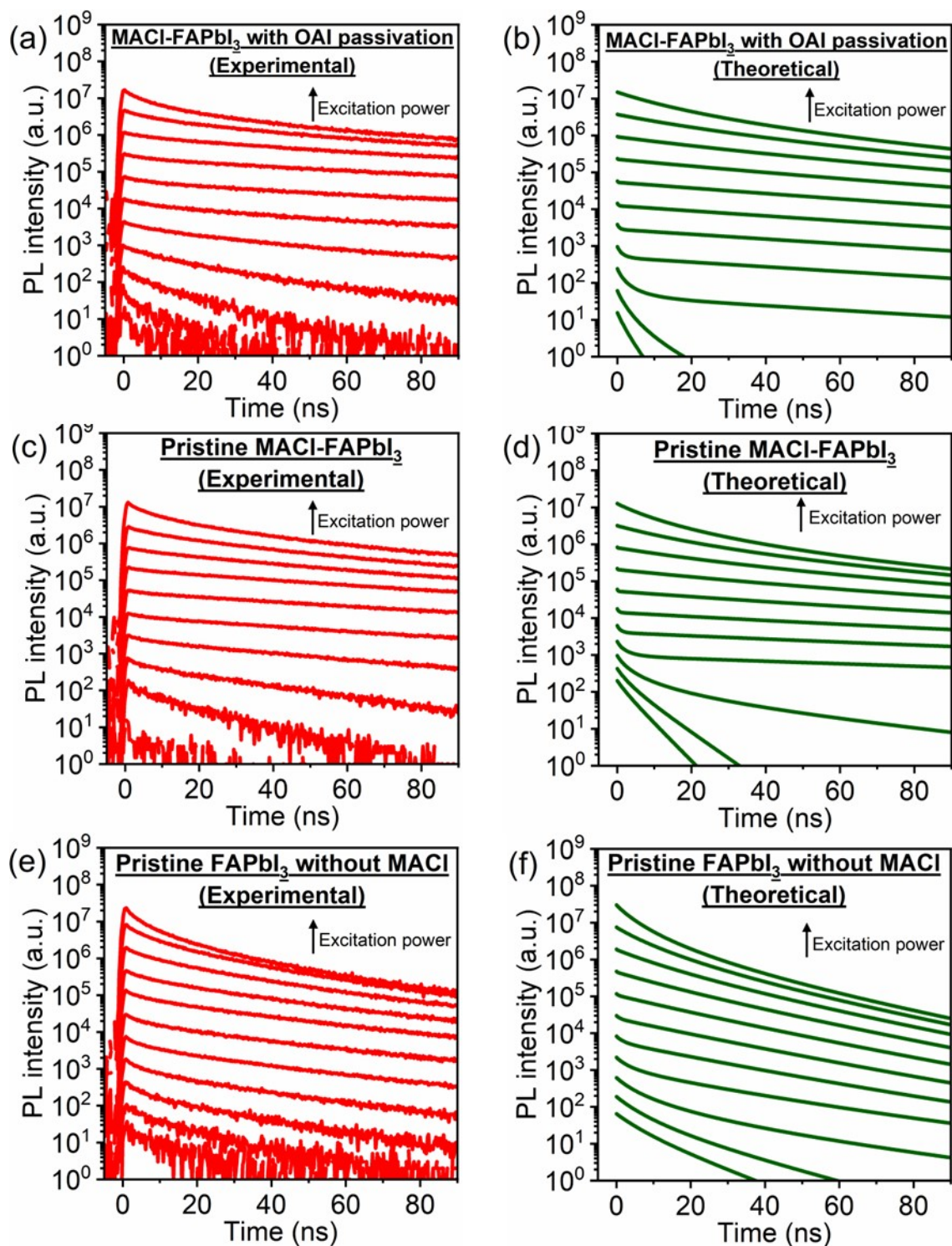
4-3. PL decays of solar cell samples

Fig. S10 Experimental and theoretical excitation power dependence on the PL decay (1–1000 nJ cm^{-2}/pulse) of solar cells comprising the photoabsorber of (a) MACl-FAPbI$_3$ with OAI passivation, (b) pristine MACl-FAPbI$_3$, and (c) pristine FAPbI$_3$ without MACl

4-4. Estimation details of kinetics parameter of the carrier injection (the C term in eq.2)

As the carrier transport materials possess considerably low mobility than perovskite materials, carrier accumulation at the interfaces of perovskite/carrier transport materials is caused with high carrier density of the perovskite photoabsorber with a strong excitation. After excitation of perovskite, this carrier accumulation occurs transiently. Thus, the *C* term in eqn 2, which represents the rate of carrier injection from perovskite to carrier transport materials, should include time-dependent term, and divided as follows:

$$C = C_1 + C_2(t) \qquad \text{(S2)}$$

$$\frac{dC_2}{dt} = -\alpha C_2 n \qquad \text{(S3)}$$

where α and *n* represent coefficient of instantaneous carrier density and carrier density, respectively.

For the fitting of the solar cell samples (Fig. 2), these equations are taken into account, and the estimated values are shown in Table S2.

Table S2. estimated values of the divided *C* term

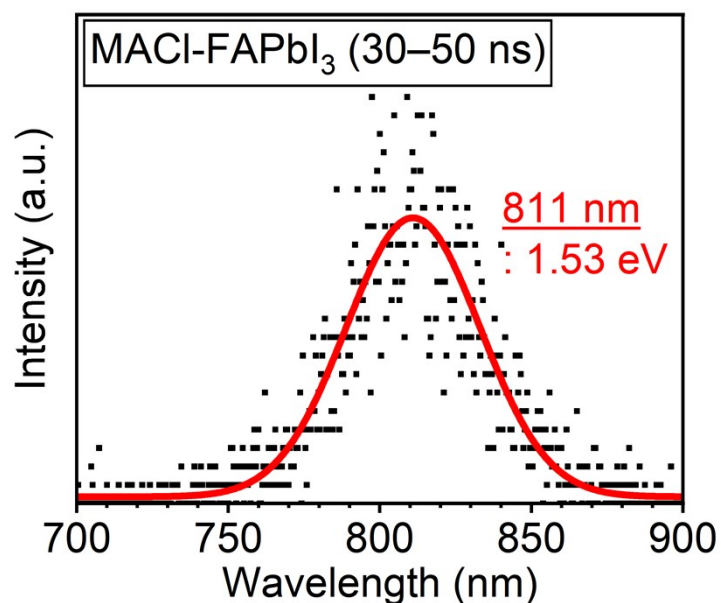| Sample	C_1 (s^{-1})	C_2 (s^{-1})	α (cm^3 s^{-1})
FAPbI$_3$-MACl with OAI passivation	7.0×10^6	2.5×10^8	8.3×10^{-8}
Pristine FAPbI$_3$-MACl	5.0×10^6	3.0×10^8	5.2×10^{-8}
Pristine FAPbI$_3$ without MACl	1.5×10^7	9.5×10^7	2.6×10^{-8}

5. Supporting data of PL spectra

Fig. S11 Fitting result of time-resolved PL spectrum of the MACl-FAPbI₃ monolayer sample in 30–50 ns (the later part); the PL peak was assigned at 811 nm: 1.53 eV
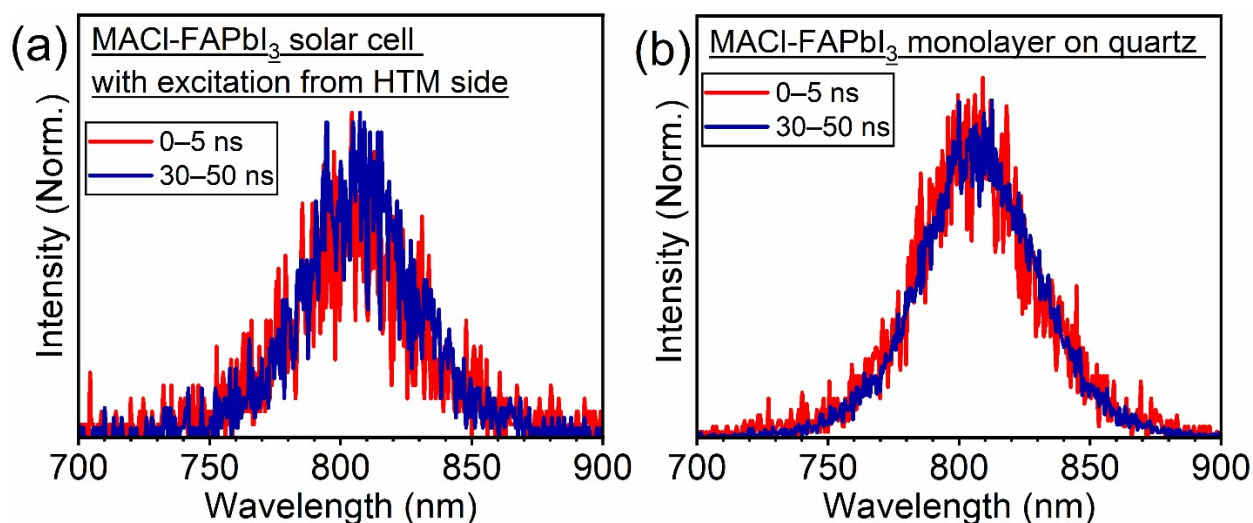

Fig. S12 Time-resolved PL spectra of (a) MACl-FAPbI₃ based solar cell excited from HTM side, (b) MACl-FAPbI₃ monolayer on quartz sample excited from the glass side.

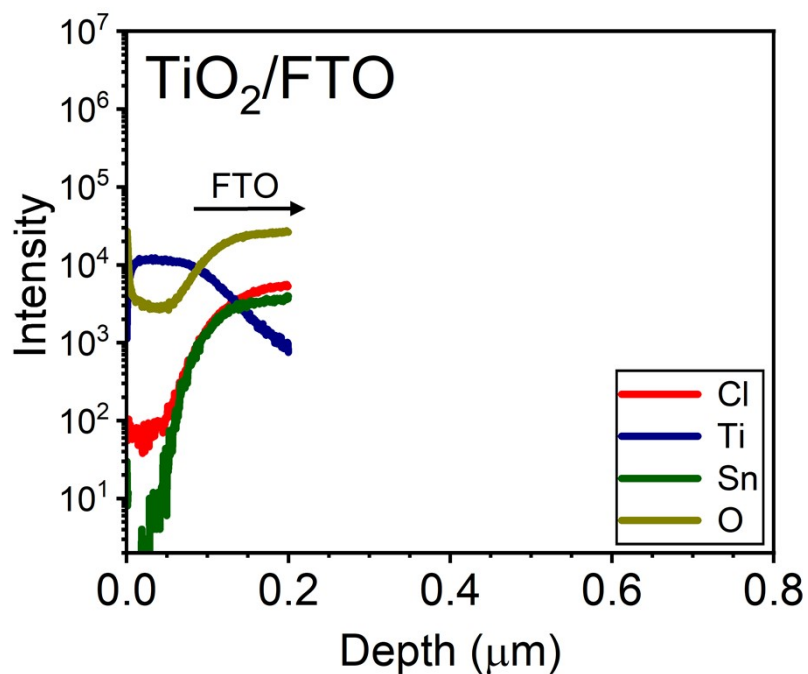## 6. Composition depth analysis of TiO$_2$/FTO reference sample

Fig. S13 Compositional depth analysis by SIMS results of TiO$_2$/ FTO reference sample

In the TiO$_2$ region of the TiO$_2$/FTO reference sample, The Cl signal that is the value similar to FAPbI$_3$ without MACl/TiO$_2$/FTO sample (Fig. 4a, approximately 50 counts) was observed. Hence, the Cl signal in the TiO$_2$ region observed in Fig. 4a was attributed to the m-TiO$_2$.

7. TRMC measurement

TRMC signal ($\Delta P/P$) is propositional to the following term:

$$\varphi \, (\mu_e + \mu_h) \qquad (S4)$$

where, φ, μ_e, and μ_h represent yield of free charges, electron mobility, and hole mobility, respectively.

[3, 5-7] Since μ_e of perovskite is significantly larger than that of TiO_2,[5] electron injection from $FAPbI_3$ to TiO_2 steeply decrease the TRMC signal of $FAPbI_3/TiO_2$ bilayer sample (Fig. S15). After the electron injection, only holes remained in $FAPbI_3$, and hence, TRMC signal decays of the bilayer sample in this work (Fig. 6c and S15b) are indicative of hole lifetime in the $FAPbI_3$ perovskite. Meanwhile, the employed excitation power for TRMC in Fig. 6 was weak (1.1 nJ/pulse) to be saturated in the excitation power dependence on TRMC decay (Fig. S14). Accordingly, in Fig. 6, bimolecular recombination between electron and hole negligibly affected the TRMC decay, and the decay was dominated by single-carrier trapping. In light of the fast time-scale electron injection (Fig. S15), therefore, the comparison of the TRMC decays between MACl-$FAPbI_3$ monolayer and eseMACl-$FAPbI_3/TiO_2$ bilayer samples is most likely indicative of whether the $FA_{1-x}MA_xPbI_{3-y}Cl_y$ interlayer derived from MACl addition acts as additional hole trapping centers. The TRMC results in the main script lead to the conclusion that the $FA_{1-x}MA_xPbI_{3-y}Cl_y$ interlayer does not act as the additional hole trapping center.
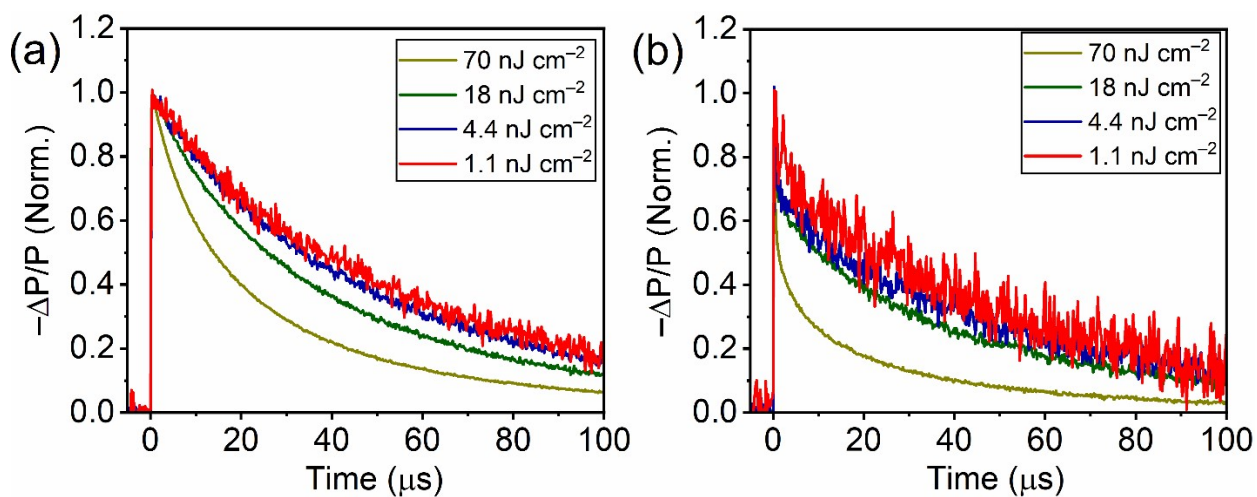
Fig. S14 Excitation intensity dependence on TRMC signals of (a) MACl-FAPbI$_3$ monolayer on quartz, (b) MACl-FAPbI$_3$/TiO$_2$ bilayer on quartz
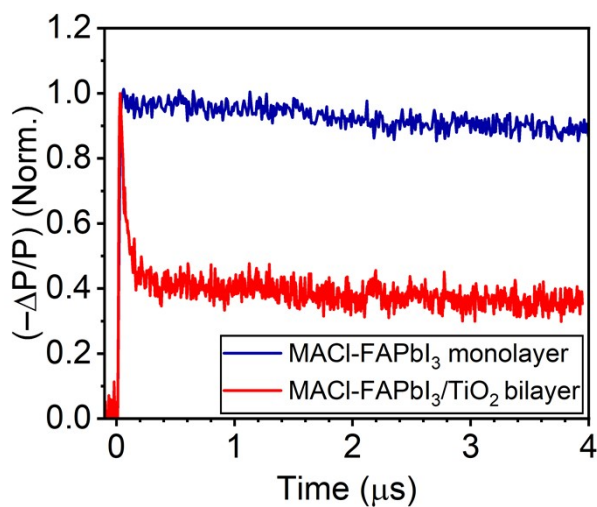

Fig. S15 TRMC decay in early stages of MACl-FAPbI$_3$ monolayer and MACl-FAPbI$_3$/TiO$_2$ bilayer

Reference

1. J. Jeong, M. Kim, J. Seo, H. Lu, P. Ahlawat, A. Mishra, Y. Yang, M. A. Hope, F. T. Eickemeyer, M. Kim, Y. J. Yoon, I. W. Choi, B. P. Darwich, S. J. Choi, Y. Jo, J. H. Lee, B. Walker, S. M. Zakeeruddin, L. Emsley, U. Rothlisberger, A. Hagfeldt, D. S. Kim, M. Gratzel and J. Y. Kim, *Nature*, 2021, **592**, 381–385.

2. N. Nishimura, S. Mathew and T. N. Murakami, *New J. Chem.*, 2023, **47**, 4197–4201.

3. N. Nishimura, H. Tachibana, R. Katoh, H. Kanda and T. N. Murakami, *ACS Appl. Mater. Interfaces*, 2023, **15**, 44859–44866.

4. A. D. Wright, G. Volonakis, J. Borchert, C. L. Davies, F. Giustino, M. B. Johnston and L. M. Herz, *Nat. Mater.*, 2020, **19**, 1201–1206.

5. H. Oga, A. Saeki, Y. Ogomi, S. Hayase and S. Seki, *J. Am. Chem. Soc.*, 2014, **136**, 13818–13825.

6. H. Hempel, T. J. Savenjie, M. Stolterfoht, J. Neu, M. Failla, V. C. Paingad, P. Kužel, E. J. Heilweil, J. A. Spies, M. Schleuning, J. Zhao, D. Friedrich, K. Schwarzburg, L. D. A. Siebbeles, P. Dörflinger, V. Dyakonov, R. Katoh, M. J. Hong, J. G. Labram, M. Monti, E. Butler-Caddle, J. Lloyd-Hughes, M. M. Taheri, J. B. Baxter, T. J. Magnanelli, S. Luo, J. M. Cardon, S. Ardo and T. Unold, *Adv. Ener. Mater.*, 2022, **12**, 2102776.

7. R. Katoh, A. Furube, K.-i. Yamanaka and T. Morikawa, *J. Phys. Chem. Lett.*, 2010, **1**, 3261–3265.